Ocean Dynamics (2003) 53: 332–342
DOI 10.1007/s10236-003-0056-5

Duncan Tippins · Matthias Tomczak

Meridional Turner angles and density compensation in the upper ocean

Received: 7 January 2003/Accepted: 18 July 2003

Abstract The World Ocean Atlas 1998 is used to determine the global field of the meridional density ratio $R_\rho^{hy} = \alpha\Delta T/\beta\Delta S$, where temperature and salinity changes ΔT and ΔS are evaluated along meridians, in and below the mixed layer. The focus of the analysis is the identification of regions where the R_ρ^{hy} field matches the values $R_\rho = 2$ sometimes suggested as the commonly perceived state of the ocean and $R_\rho = 1$, the condition of density compensation. Results are presented through fields of the meridional Turner angle $Tu^{hy} = \arctan(R_\rho^{hy})$ and through histograms of Tu^{hy} for the Pacific, Atlantic and Indian Oceans at the ocean surface and at 300 m depth. At the 300-m depth level, which in the subtropics is representative of conditions in the permanent thermocline, the most frequently encountered values of the meridional density ratio are $R_\rho^{hy} = 3.2$ in the North and South Pacific, $R_\rho^{hy} = 2.0$ in the South Atlantic and Indian and $R_\rho^{hy} = 1.6$ in the North Atlantic Ocean. Conditions in the mixed layer are more variable and show seasonal differences, but $R_\rho^{hy} = 2.0$ occurs prominently in all ocean regions during winter and in all regions but the Atlantic during summer. Summer values for the Atlantic Ocean are $R_\rho^{hy} = 3.2$ in the Northern Hemisphere and $R_\rho^{hy} = 2.4$ in the Southern Hemisphere. Detailed analysis of R_ρ^{hy} across the Subtropical Front (STF) confirms the most frequently observed values but shows zonal variation along the front in some oceans. Nearly complete density compensation ($R_\rho^{hy} = 1$) in the mixed layer is encountered in the STF of the eastern North Pacific, the eastern South Pacific and the eastern Indian Ocean. The eastern Indian Ocean south of Australia is also the only region where complete density compensation in the STF occurs below the mixed layer.

Keywords Turner angle · Density compensation · Subtropical front

Responsible Editor: Neville Smith

D. Tippins (✉)
Bureau of Meteorology,
GPO Box 1289K, Melbourne VIC. 3001, Australia
e-mail: d.tippins@bom.gov.au
Tel.: +61-8-8366-2796
Fax: +61-8-8366-2683

M. Tomczak
School of Chemistry Physics and Earth Science,
Flinders University, GPO Box 2100,
Adelaide SA, 5001, Australia

1 Introduction

The ocean and the atmosphere are fluids in turbulent motion, and their dynamical behaviour is similar in many respects. One of the major differences between the two media is the possibility of density compensation in the ocean: while the density of the atmosphere is controlled essentially by its temperature and pressure, with some influence from its moisture content, the ocean's density field is controlled by temperature, pressure and salinity. In the ocean, the density effect of salinity variations can, on occasion, neutralize the density effect of temperature variations, leading to a situation of no change in density even in the presence of substantial temperature and salinity changes.

The dynamic consequences of density compensation are most clearly felt in oceanic fronts. Atmospheric fronts are invariably density fronts (Gordon et al. 1998) and thus accompanied by stronger winds along the front and enhanced turbulence and eddy formation in the frontal zone. Oceanic fronts have very similar dynamics, as long as they are associated with a significant density gradient. Density-compensated fronts, on the other hand, are a unique feature of the ocean. They are seen as well-established temperature and salinity fronts but have only a very weak density signature (Roden 1975). As a consequence, they are not associated with strong geostrophic flow, and mixing in the frontal zone is dominated by interleaving on density surfaces and by double diffusive processes.

Although observations of density compensation have been reported for several decades, a clear explanation

why density compensation should be a preferred state of the ocean for scales larger than the Rossby deformation radius is still lacking. A key parameter for the analysis is the density ratio $R_\rho = \alpha\Delta T/\beta\Delta S$, where $\alpha = -1/\rho\partial\rho/\partial T$ is the thermal expansion coefficient and $\beta = 1/\rho\partial\rho/\partial S$ the haline contraction coefficient (ρ is the seawater density). In most applications ΔT and ΔS are evaluated as vertical gradients. R_ρ is then a measure of the relative contributions of temperature and salinity to the stratification. The same quantity can be used to quantify the degree of density compensation across oceanic fronts or in the surface mixed layer if ΔT and ΔS are evaluated as horizontal gradients. To avoid ambiguity, we denote the density ratio as R_ρ^h when it is evaluated in the horizontal and as R_ρ^v when it is evaluated in the vertical. In both cases the condition for complete density compensation is given by $R_\rho = 1$.

Stommel (1993) proposed that atmospherically driven random fluctuations of temperature and salinity can result in horizontal property fluxes that drive the mixed layer towards a state of constant $R_\rho^h = 2$. This would indicate a dominance of temperature over salinity in the density field of the surface layer and, by inference through the subduction mechanism, produce a constant $R_\rho^v = 2$ for the oceanic thermocline.

Stommel's result $R_\rho^h = 2$ is not supported by observations of TS variability on scales smaller than 10 km, which often indicate perfect density compensation (Rudnick and Martin 2002). Ferrari and Young (1997) and Rudnick and Ferrari (1999) put forward theoretical arguments that support $R_\rho^h = 1$ in the mixed layer for these small scales, but the relevant scale for Stommel's analysis is oceanic scales of several hundreds of kilometres, where the evidence is more ambiguous and $R_\rho^h = 2$ is often accepted as a good description of the meridional variation of temperature and salinity in the subtropics (Schmitt 1999).

There is evidence to suggest that the universal rule of $R_\rho^h = 2$ for the oceanic thermocline does not hold on regional scales or across dynamical boundaries, such as the boundary between the South Equatorial Current and the Equatorial Undercurrent (Tomczak and Gu 1987). A comparison of different ocean basins also indicates different values of R_ρ^h for different oceans (Figueroa 1996). Because subduction in the Subtropical Convergence effectively translates any R_ρ^h relationship into an R_ρ^v relationship, it can be anticipated that the same relationships found for R_ρ^v in different oceans should also be found in meridional R_ρ^h relationships below the surface mixed layer. To increase the observational evidence for or against density compensation or other $R_\rho^h =$ constant relationships, it seems worth while to investigate and compare the R_ρ^h fields in the mixed layer and at some depth below this layer.

This study evaluates R_ρ^h in and below the mixed layer for the global ocean for the summer and winter periods. It focuses in particular on the Subtropical Fronts as regions of potential density compensation. The aim is to provide observational information to assist theoretical initiatives that try to find the dynamic link between properties of the oceanic mixed layer and the properties of the thermocline. Its results reveal similarities between all three subtropical oceans but also significant variations of R_ρ^h within and between different ocean basins.

2 Data and methods

The basis for the present analysis is the World Ocean Atlas 1998 (Conkright et al. 1998). This electronic atlas, available on CD-ROM, allows the selection of objectively analyzed gridded hydrographic data sorted by months and seasons with a grid size of 1° latitude by 1° longitude. Its seasons are defined as summer: July–September, autumn: October–December, winter: January–March, spring: April–June. The objective analysis applies smoothing over roughly 500 km and so the analysis here is applicable only to variations over comparable distances. At this scale the noise inherent in individual profiles has been removed by the objective analysis. Fields of data distribution, standard error of the mean and standard deviation are available on the CD-ROM along with the analyzed fields.

We present here the analysis for the summer and winter seasons but avoid the terms summer for July–September and winter for January–March because they are misleading for most of the ocean (which is in the Southern Hemisphere).

Although R_ρ is the most important physical parameter for processes influenced by the degree of density compensation (for example double diffusion), its nonlinear dependence on ΔS makes R_ρ not a convenient descriptor of the prevailing oceanic conditions. A better measure of the degree of density compensation is the Turner angle Tu defined by Ruddick (1983) as:

$$Tu = \arctan\left(\frac{\alpha\Delta T - \beta\Delta S}{\alpha\Delta T + \beta\Delta S}\right).$$

Thus defined, the Turner angle is $\pm$ 90° when density compensation is complete and $> |90°|$ for statically impossible (unstable) stratifications.

Ruddick's definition was introduced for the analysis of vertical temperature and salinity profiles, so ΔT and ΔS are the changes in temperature and salinity over a fixed vertical distance. In the present context, his Turner angle may therefore be denoted by Tu^v. The choice of the vertical coordinate excludes half the possible range of Tu^v from occurring in oceanic situations. We introduce the equivalent quantity, Tu^h, the horizontal Turner angle, by defining ΔT and ΔS as the temperature and salinity changes observed in the horizontal direction. Because ocean physics places no restriction on possible $\Delta T/\Delta S$ combinations on horizontal surfaces, Tu^h can have any value.

To highlight the difference between Tu^v and Tu^h, we define the horizontal Turner angle through

$$Tu^h = \arctan\left(\frac{\alpha\Delta T}{\beta\Delta S}\right),$$

with ΔT and ΔS now horizontal changes of the two properties. In the analysis of this paper they are evaluated along meridians (the y-coordinate of the usual oceanographic coordinate system). We refer to the thus defined angle as the meridional Turner angle Tu^{hy}. Figure 1 compares the two definitions Tu^{v} and Tu^{hy}. Complete density compensation in the horizontal is indicated by $Tu^{hy} = 45°$, while a preferred value of $R_\rho^h = 2$ corresponds to a meridional Turner angle of $Tu^{hy} = 63.4°$.

Frequency histograms of the meridional Turner angle on horizontal surfaces were prepared for individual ocean regions by counting the occurrences of Tu^{hy} values in bins of 5°. Longitude convergence has the consequence that $1° \times 1°$ squares decrease in area towards the pole. Therefore, to have the $1° \times 1°$ squares comparable to a square at the equator, the counts were multiplied by the cosine of their latitude. In addition, the different oceans vary substantially in area. To allow for an objective comparison between them, the histograms were normalized by dividing by each basin's total count.

3 Global distribution of the meridional Turner angle

Figures 2 and 3 present a global overview of Tu^{hy} for the sea surface and for 300 m depth. This depth level is deep enough to be beneath the mixed layer during all seasons over most of the subtropics, yet shallow enough to be located entirely in the permanent thermocline, even in the tropics.

In the polar and subpolar regions, which do not concern us in the present analysis, the meridional Turner angle is close to zero, a consequence of the near-zero values of the thermal expansion coefficient at low temperatures. In the remainder of the world ocean the two depth surfaces show a distinctly different structure.

At the surface (Fig. 2) Tu^{hy} is positive between the Subpolar Front and the centre of the subtropics, indicating that temperature and salinity both increase towards the Equator. Closer to the equator the temperature continues to increase but the meridional salinity gradient is reversed on the equatorial side of the subtropical surface salinity maximum; as a consequence, the meridional Turner angle becomes negative. Reduced temperatures from equatorial upwelling change the sign of the meridional temperature gradient, and Tu^{hy} becomes positive again in the Pacific and Atlantic Oceans near the equator. A band of negative Tu^{hy} in the South Pacific stretches westward along 45°S, produced by the rainfall-induced low salinities off the southern coast of Chile.

In contrast, the 300-m level (Fig. 3) is dominated by positive Tu^{hy} nearly everywhere between the Subpolar

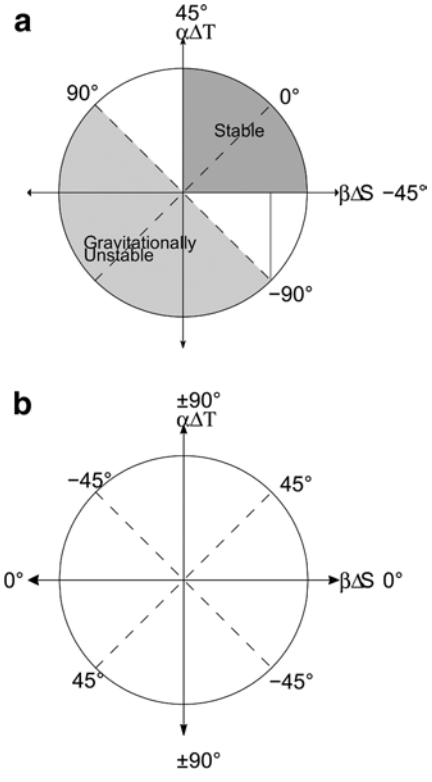

Fig. 1 A comparison of the possible ranges for the vertical Turner angle Tu^{v} and the meridional Turner angle Tu^{hy}. The meridional Turner angle is measured counterclockwise from the $\beta\Delta S$ axis. Complete density compensation is indicated by $Tu^{v} = \pm\ 90°$ and by $Tu^{hy} = 45°$

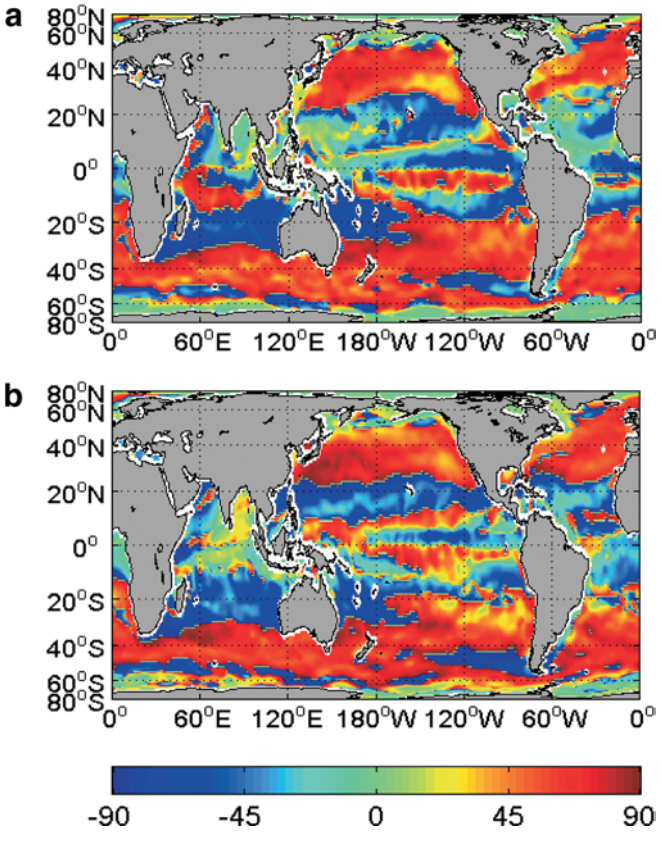

Fig. 2a, b Global distribution of the meridional Turner angle Tu^{hy} at the sea surface. **a** July–September, **b** January–March, in Gall–Peters projection

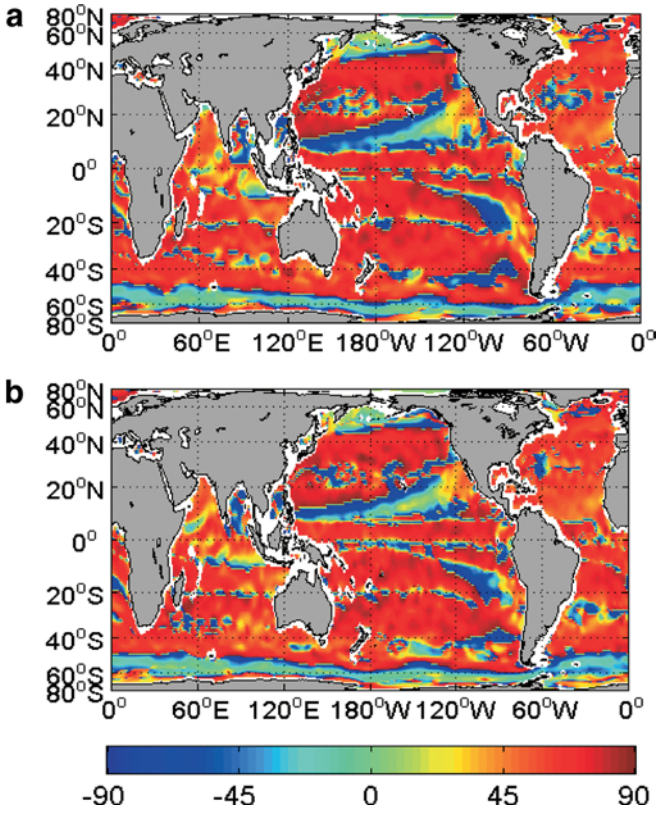

Fig. 3a, b Global distribution of the meridional Turner angle Tu^{hy} at 300 m depth. **a** July–September, **b** January–March, in Gall–Peters projection

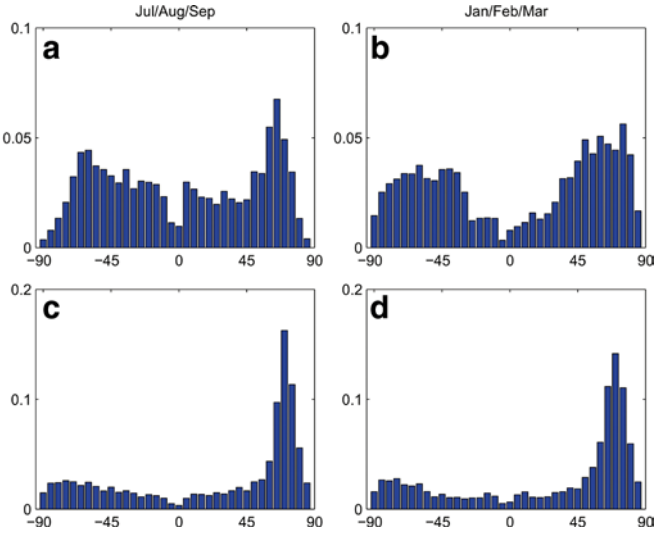

Fig. 4a–d Normalized histograms of the meridional Turner angle Tu^{hy} for the North Pacific Ocean. **a** Surface, July–September. **b** Surface, January–March. **c** 300 m, July–September. **d** 300 m, January–March

Fronts and shows only narrow bands of negative Turner angles. This reflects the shape of the permanent thermocline, which sinks to its greatest depth in the centre of the oceanic gyres and then rises again towards the equator. Central water, the water mass of the permanent thermocline, is characterized by a vertical structure in which temperature and salinity both decrease with depth. A traverse of the gyres at constant depth from the poleward side towards the equator therefore begins with an increase in temperature and salinity as the thermocline moves to greater depth. Once its greatest depth is reached and the thermocline starts to rise, both temperature and salinity decrease again towards the Equator. Both situations produce a positive R_ρ^{hy} and thus a positive Tu^{hy}. The location of the greatest thermocline depth, where ΔS changes sign and $\alpha\Delta T/\beta\Delta S$ goes to infinity, is indicated by the narrow bands of large negative Turner angles.

Superimposed on these basin-scale trends in the distribution of Tu^{hy} are regional and interbasin variations of significant magnitude. To investigate these additional variations of Tu^{hy}, we present Tu^{hy} frequency histograms for individual oceans and seasons.

First derivative quantities such as ΔT and ΔS are inherently noisy. The histograms show this noise as a data spread around physically significant values. Where sufficient data are available, accepting significant noise in the histogram is preferable over additional smoothing of the data, which would reduce peak gradients. All histograms are therefore based on the original 1°-square grid size of the atlas.

Figure 4 shows normalized Tu^{hy} histograms for the North Pacific Ocean. As expected from Fig. 2, the surface distribution is bimodal, with peaks in the bins centred on 62.5° and −57.5°. The positive mode represents the subtropics poleward of the surface salinity maximum, the negative mode the subtropics on the equatorward side. The peak of the negative mode is quite broad and, particularly in summer, the number of occurrences of values near −62.5° is barely less than the peak value at −57.5°. The positive mode confirms the dominance of $R_\rho^{hy} = 2$ ($Tu^{hy} = 63.4°$) in the mixed layer on scales exceeding 100 km.

In comparison, the distribution at the 300-m level shows the clear preference expected from Fig. 3 for positive Tu^{hy} values. Most of the negative Tu^{hy} values are found in the Arctic region, where the 1°-square area is small. The histogram shows a well-defined peak centred on 72.5° or a stability ratio of $R_\rho^{hy} = 3.2$.

Figure 5 gives the same information for the South Pacific Ocean. The general shape of the histograms is similar to those for the North Pacific. The surface histograms are again bimodal with a peak at 62.5°. The peak in the negative range occurs at −82.5° in January–March (summer) and in the range −65° to −80° in July–September (winter). At the 300-m level the distribution is again dominated by the positive range and peaks at 72.5°.

The situation for the Atlantic Ocean is shown in Figs. 6 and 7. The bimodal surface distribution of the North Atlantic shows peaks at 72.5° and −10° in July–September (summer) and at 62.5° and −37.5° in January–March (winter). The positive summer peak is

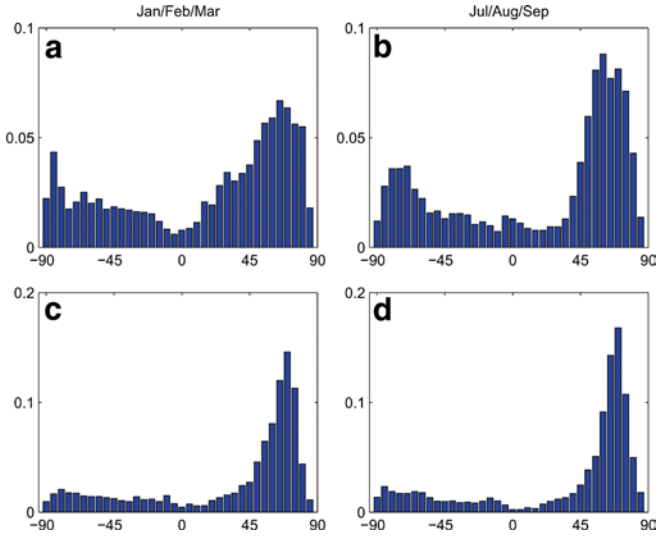

Fig. 5a–d Normalized histograms of the meridional Turner angle Tu^{hy} for the South Pacific Ocean. **a** Surface, January–March. **b** Surface, July–September, **c** 300 m, January–March. **d** 300 m, July–September

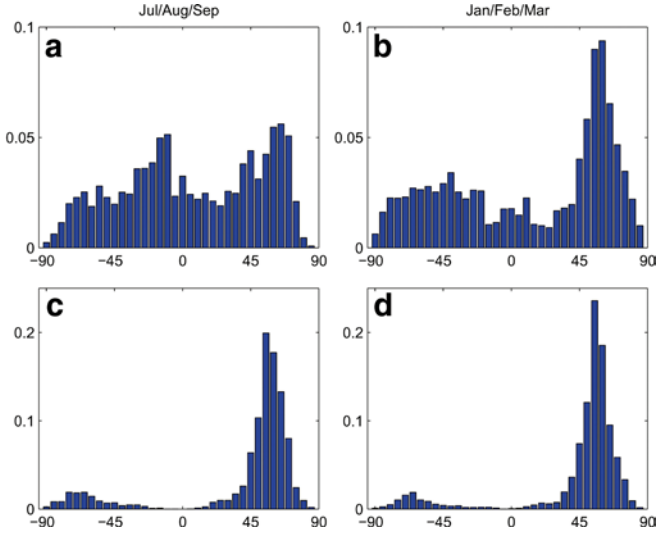

Fig. 6a–d Normalized histograms of the meridional Turner angle Tu^{hy} for the North Atlantic Ocean. **a** Surface, July–September. **b** Surface, January–March. **c** 300 m, July–September. **d** 300 m, January–March

relatively broad and unlikely to have an impact on the climatological structure of the thermocline, as winter mixing will erase its signature before it can influence deeper layers. The positive winter peak indicates a transformation of Tu^{hy} values over most of the North Atlantic towards 62.5°, again confirming the dominance of $R_\rho^{hy} = 2$ for the mixed layer.

At the 300-m level nearly all Tu^{hy} values in the North Atlantic are found in the positive range but peak at 57.5°, which corresponds to a stability ratio of $R_\rho^{hy} = 1.6$.

A similar situation is observed in the South Atlantic Ocean. At the surface the histogram shows again a narrow positive range with a sharp peak at 62.5° during

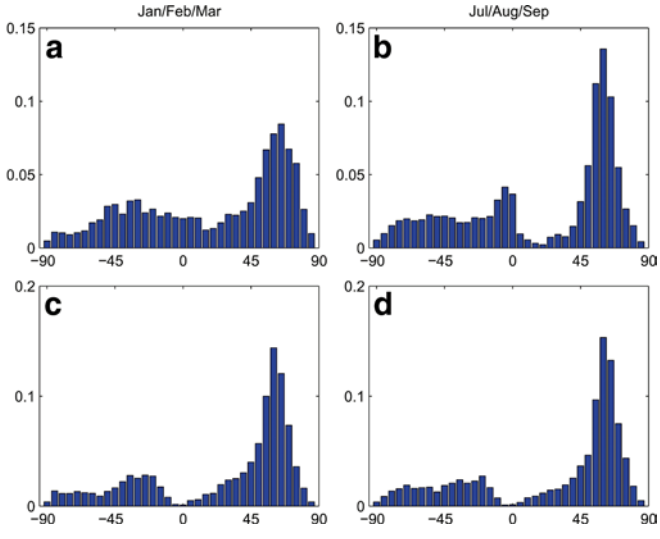

Fig. 7a–d Normalized histograms of the meridional Turner angle Tu^{hy} for the South Atlantic Ocean. **a** Surface, January–March. **b** Surface, July–September. **c** 300 m, January–March. **d** 300 m, July–September

winter (July–September), while the broader summer (January–March) peak is found at higher Turner angle values (67.5°). At 300 m depth a relatively large proportion of the histogram is occupied by negative Turner angles, mainly of Antarctic origin. The peak in the positive range is stable over the seasons and found at 62.5° or $R_\rho^{hy} = 2$.

The Indian Ocean is closed towards the north and does not reach far enough north to allow water mass formation of any large extent in the Northern Hemisphere. The water masses of the permanent thermocline are therefore ventilated from the Southern Hemisphere (You and Tomczak 1993). In the present context it is sufficient to restrict the analysis to the Southern Indian Ocean (Fig. 8).

The histogram for the surface layer shows a trimodal distribution with slightly changing peak angles for the different seasons. During January–March (summer) clear peaks are found at 62.5° and −67.5°, although the latter is broad and could be anywhere in the range −52.5° to −72.5°. A shallow rise with no distinct peak is located between −20° and + 12.5°. During winter (July–September) the same peaks are found at 57. 5° to 62. 5° and at −72.5°, and the shallow rise has risen into a peak at 12. 5°. This region of small Turner angles is the contribution from the Southern Ocean. It is present in all Southern Hemisphere distributions but becomes more prominent here because of the relatively small size of the southern Indian Ocean.

The histogram for the 300-m level is again dominated by positive Turner angles. The peak is located at 62.5° ($R_\rho^{hy} = 2$) throughout the year. There is an indication of a seasonal broadening of the histogram during winter (July–September).

Table 1 summarizes the results of the histogram analysis. It is seen that on scales larger than 500 km,

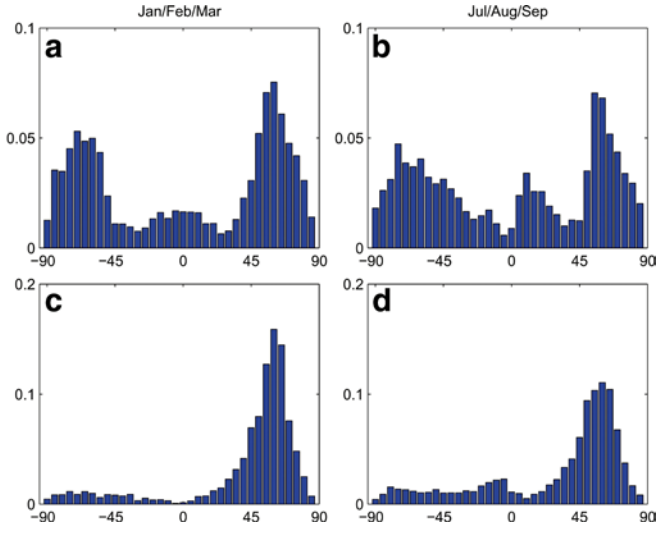

Fig. 8a–d Normalized histograms of the meridional Turner angle Tu^{hy} for the South Indian Ocean. **a** Surface, January–March. **b** Surface, July–September. **c** 300 m, January–March. **d** 300 m, July–September

density compensation is not the most frequent state of the ocean. Nevertheless, the histograms of all oceans display a wide range of Tu^{hy}, and the area of ocean where Tu^{hy} values of $+45°$ are encountered particularly in the mixed layer is not insignificant. To investigate the possible occurrence of density compensation, we proceed to an analysis of the meridional Turner angle across the Subtropical Front.

4 Density compensation across the Subtropical Front

The location of the Subtropical Front (STF) was derived from the literature. Tu^{hy} was calculated by determining ΔT and ΔS from meridional differences between groups of three adjacent 1°-squares centred on the front. In order to reduce the noise inherent in first derivative quantities, the result was averaged over the three squares and thus represents conditions at the front on cross-front scales of 500 km or more.

Figure 9 gives the meridional Turner angle across the STF in the North Pacific Ocean. The position of the STF was taken from Roden (1975) and Tomczak and Godfrey (1994). At the 300-m level the STF follows the most frequent North Pacific value of $Tu^{hy} = 72.5°$ ($R_\rho^{hy} = 3.2$) very closely. At the surface the average Tu^{hy} value along the STF corresponds to the most frequent value of $Tu^{hy} = 63.4°$ ($R_\rho^{hy} = 2.0$; here and in the following we assume that, given the histogram resolution of 5°, a peak centred on 62.5° indicates the value $R_\rho^{hy} = 2$ suggested in the literature, which corresponds to $Tu^{hy} = 63.4°$); but a clear zonal variation of Tu^{hy} is obvious. East of 165 °W to about 700 km off the American coast the values come closer to density compensation during summer; during the winter this region is reduced to a small area at 130°–140°W.

The situation for the STF in the South Pacific is shown in Fig. 10. The position of the front is based on Kazmin and Rienecker (1996). The situation is very similar to the situation found in the North Pacific. At 300 m depth the Tu^{hy} values follow the most frequent Pacific value of $Tu^{hy} = 72.5°$ ($R_\rho^{hy} = 3.2$), the exception being the region in the east where Tu^{hy} oscillates between $+90$ and $-90°$. At the surface there is again a trend from large values in the west towards density compensation in the east. East of 100°W Tu^{hy} values fall well below 45° during summer (January–March), indicating that the meridional density gradient is then dominated by the salinity.

In comparison, the Atlantic Ocean presents rather uniform conditions where a Subtropical Front is present. The North Atlantic Ocean (Fig. 11) is characterized by widespread deep winter convection, and a clear

Table 1 Area-weighted most frequently observed meridional Turner angles and stability ratios. *s* summer; *w* winter (as defined for the respective hemispheres). *Where no season is given* the value applies to both seasons

Ocean	Surface		300 m	
	Tu^{hy}(°)	R_ρ^h	Tu^{hy}(°)	R_ρ^h
North Pacific	62.5	2.0	72.5	3.2
	−57.5 to −62.5	1.6–2.0		
South Pacific	62.5	2.0	72.5	3.2
	−82.5 (s)	7.6		
	−65 to −80 (w)	2.1–5.7		
North Atlantic	72.5 (s)	3.2	57.5	1.6
	−10 (s)	0.2		
	62.5 (w)	2.0		
	−27.5 to −37.5 (w)	0.8		
South Atlantic	67.5 (s)	2.4	62.5	2.0
	−2.5 (s)	> 0.0		
	62.5 (w)	2.0		
	−27.5 to −37.5 (w)	0.5–0.8		
South Indian	57.5 to 62.5 (w)	1.6–2.0	62.5	2.0
	−72.5 (w)	3.2		
	12.5	0.2		
	62.5 (s)	2.0		
	−52.5 to −72.5 (s)	1.3–3.2		
	−20 to + 12.5 (s)	0.2–0.4		

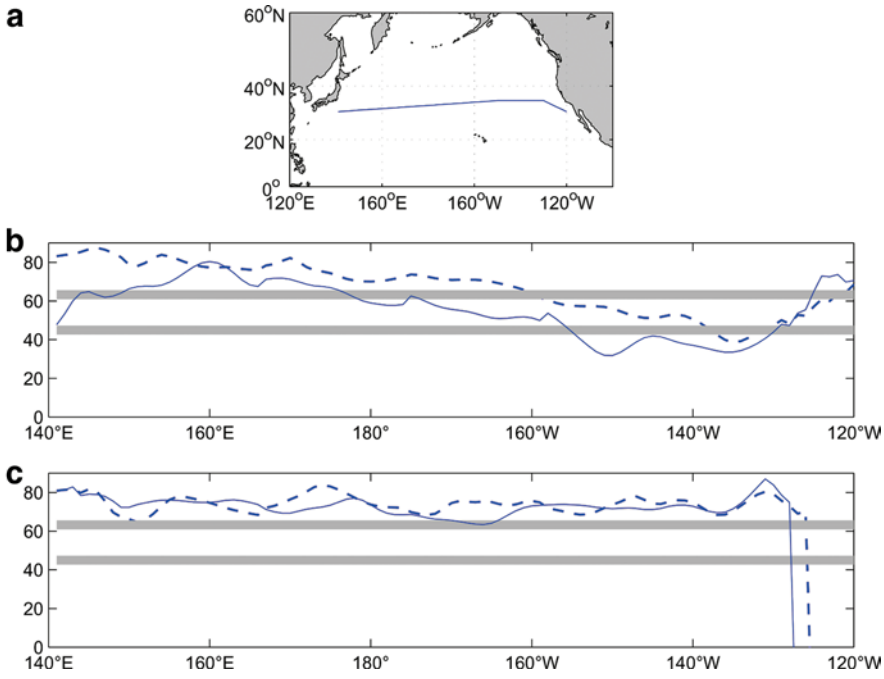

Fig. 9a–c The meridional Turner angle as a function of longitude along the Subtropical Front of the North Pacific. **a** Location of the front. **b** Surface. **c** 300 m. The *solid line* is for July–September (summer), the *broken line* for January–March (winter). *Horizontal bands* indicate the Turner angle values for complete density compensation ($Tu^{hy} = 45°$, $R_\rho^h = 1$) and for the "canonical value" $R_\rho^h = 2$ ($Tu^{hy} = 63.4°$). The *width of the bands* corresponds to the 5°-resolution of the histograms

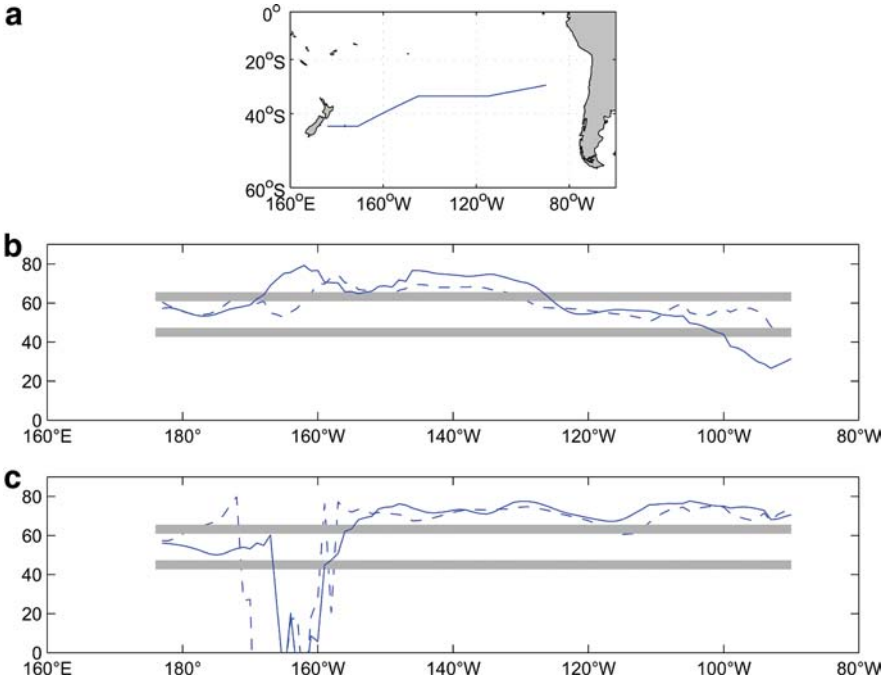

Fig. 10 As Fig. 9, but for the South Pacific Ocean. The *solid line* is for January–March (summer), the *broken line* for July–September (winter)

subtropical front is restricted to the eastern regions, where it is known as the Azores Front. Its location was derived from Tomczak and Godfrey (1994). Tu^{hy} values at 300 m depth over this relatively short stretch of front do not follow the most frequent North Atlantic values of $Tu^{hy} = 57.5°$ ($R_\rho^{hy} = 1.6$) but are closer to the "canonical" value of $Tu^{hy} = 63.4°$ ($R_\rho^{hy} = 2$). This value is, however, found at the surface during winter and for most of the front also during summer.

The position of the STF in the South Atlantic Ocean (Fig. 12) is based on Belkin and Gordon (1996) and on Tomczak and Godfrey (1994). This front is well defined from South America to South Africa. At 300 m depth its Tu^{hy} values are close to $Tu^{hy} = 63.4°$ ($R_\rho^{hy} = 2$); as in all other oceans, they do not vary seasonally. Values at the surface show some variation between summer (July–September) and winter (January–March) east of 20°W, where Tu^{hy} attains the most frequent South Atlantic value for the respective seasons ($Tu^{hy} = 67.5°$ ($R_\rho^{hy} = 2.4$) during summer, $Tu^{hy} = 63.4°$ ($R_\rho^{hy} = 2$) during winter). West of 20°W a value of $Tu^{hy} = 63.4°$ ($R_\rho^{hy} = 2$) is maintained throughout the year. Conditions

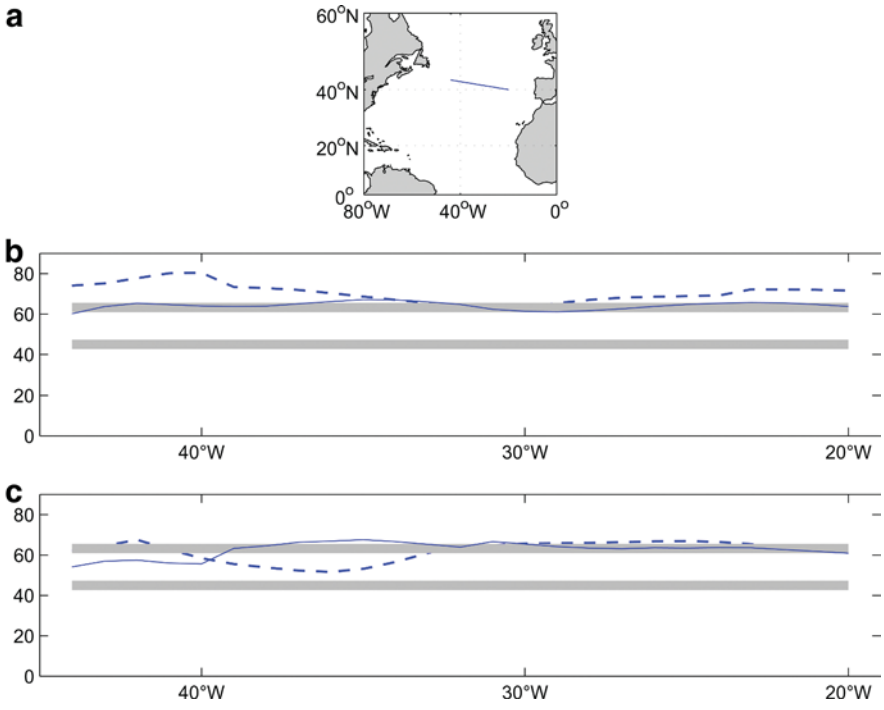

Fig. 11 As Fig. 9, but for the North Atlantic Ocean. The *solid line* is for July–September (summer), the *broken line* for January–March (winter)

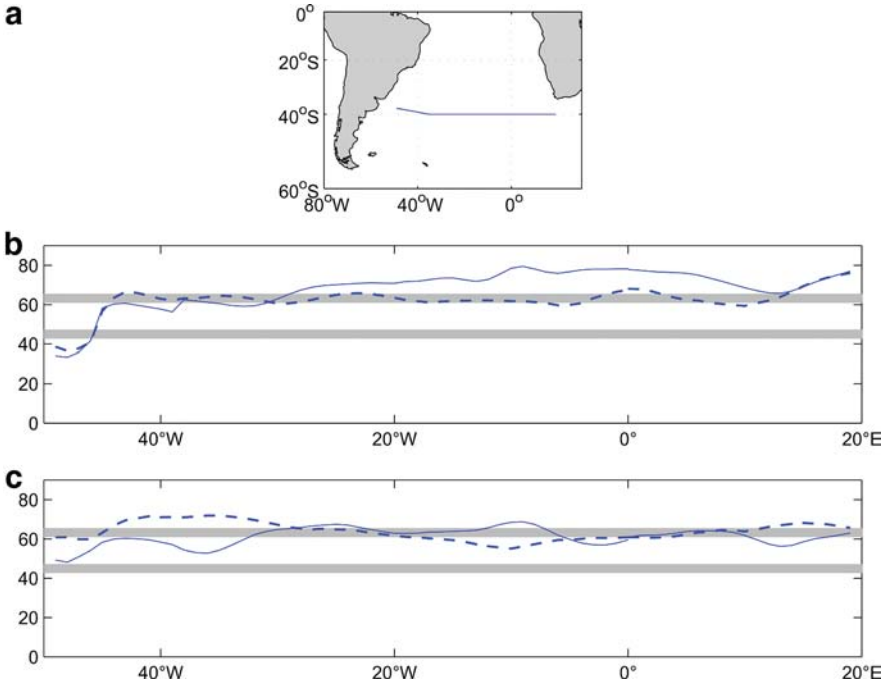

Fig. 12 As Fig. 9, but for the South Atlantic Ocean. The *solid line* is for January–March (summer), the *broken line* for July–September (winter)

of density compensation are not found anywhere at the STF of the Atlantic Ocean in both hemispheres.

The Indian Ocean is the only ocean region where density compensation is observed at the 300-m level. The position of the STF was determined from Belkin and Gordon (1996) and from James et al. (2002). Its meridional Turner angle shows significant spatial variation, particularly in the east and south of Australia (Fig. 13), but this could be a result of sparse sampling and therefore the gridded dataset may be somewhat uneven. At 300 m depth Tu^{hy} west of 90°E is close to but somewhat smaller than $Tu^{hy} = 63.4°$ ($R_\rho^{hy} = 2$). East of 90°E Tu^{hy} drops off to lower values and reaches values indicative of complete density compensation during summer at some locations. Tu^{hy} values at the surface generally follow $Tu^{hy} = 63.4°$ ($R_\rho^{hy} = 2$), the most frequent value for the Indian Ocean, but fall off towards complete density compensation during winter between 80°E and 100°E.

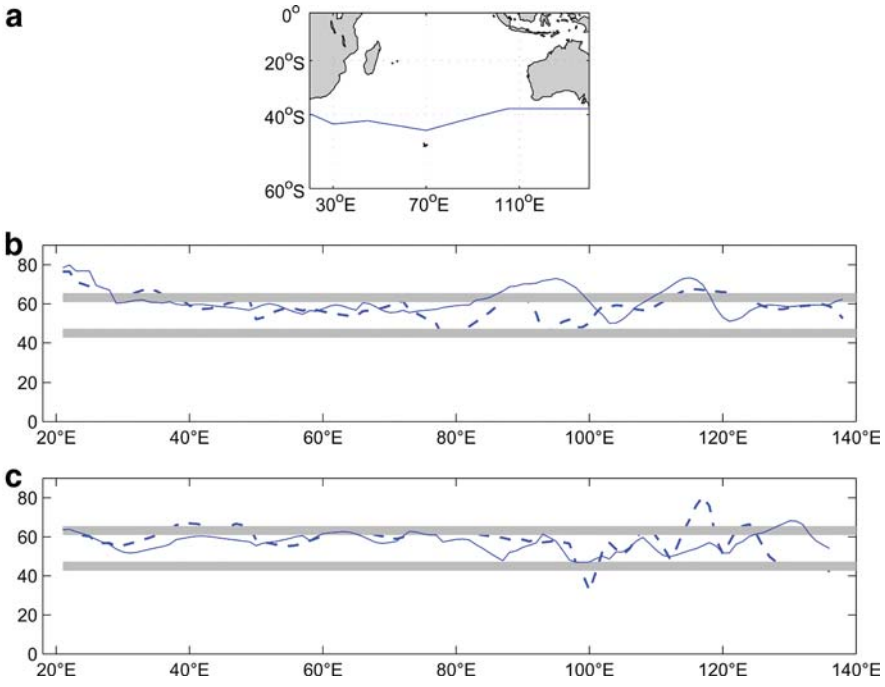

Fig. 13 As Fig. 9, but for the South Indian Ocean. The *solid line* is for January–March (summer), the *broken line* for July–September (winter)

5 Discussion

The intention of this study was to provide observational information that can assist theoretical initiatives to find the dynamic link between properties of the oceanic mixed layer and the properties of the thermocline. The study extends the work of Chen (1995), who used the Levitus (1982) dataset for a global analysis of the meridional density ratio in the mixed layer. Most of Chen's analysis was based on annual mean sea-surface temperature and salinity distributions; it was also restricted to the mixed layer and did not address the underlying thermocline. The only histogram of density ratios in his work did not differentiate between different ocean basins but used the global dataset. The most detailed results were given for the North Pacific Ocean, for which Chen provided density ratios for annual mean and winter mean data as functions of longitude. Chen's findings for the North Pacific Ocean are in good agreement with the findings of the present study.

Other work on horizontal density ratios focuses on much smaller scales. On smaller time and space scales density compensation is a well-known feature of the oceanic mixed layer, where vertical temperature and salinity gradients are negligible but horizontal gradients can be substantial, resulting from spatial differences in rainfall and solar heating. It is a common observation that patches of low salinity show a drop in temperature just large enough to cancel the density effect of the salinity (Roden 1980a). Temperature-salinity (*TS*) diagrams produced from thermosalinograph records often show the data aligned on constant density surfaces (Tomczak 1977).

Rudnick and Ferrari (1999) found that the mixed layer in the eastern North Pacific is horizontally density-compensated on scales smaller than the Rossby radius of deformation (about 10 km), but suspected that their finding that density compensation was also seen at larger scales was special to the area. In a more recent study, Rudnick and Martin (2002) use SeaSoar data from various ocean basins to analyze scales of about 3–4 km and draw conclusions on the global distribution of the horizontal density ratio at that scale. Their results show a clear tendency for the horizontal density ratio to change from values close to 1 in the mixed layer to values close to 2 below the mixed layer. Whether their data coverage in space and time is good enough to allow conclusions on global distributions might well be questioned (their dataset does not include any observations from the Southern Hemisphere at all), but on scales of 1–10 km it is conceivable that local processes, which are the same everywhere in the upper ocean, are more important than large-scale atmospheric forcing that differs from basin to basin, and that a limited dataset can produce results of general applicability.

Observations of density compensation in oceanic fronts have been frequently reported, including from the Subtropical Front of the Northern (Roden 1980b; Niiler and Reynolds 1984; Yuan and Talley 1992) and Southern Hemisphere (James et al. 2002), from the Subantarctic Front in the Atlantic sector (Roden 1986) and from the Subarctic Front of the Pacific (Roden 1977; Yuan and Talley 1992).

Our findings indicate that the STF of the North Pacific tends towards density compensation east of 165°W. This confirms that the region between 25–35° N along 140°W studied by Rudnick and Ferrari (1999) is indeed

one of the few regions displaying density compensation in the surface layer at scales that exceed the Rossby deformation radius. It has to be kept in mind that the World Ocean Atlas scale is 1° in latitude and longitude and that even on that scale the data are averaged over about 500 km. The temperature and salinity gradients used in this paper are therefore true descriptors of large-scale phenomena.

The other two regions where the STF is near density compensation in the mixed layer are the eastern South Pacific east of 100°W and the eastern Indian Ocean southwest of Australia. The result for the Indian Ocean is supported by the observational work of James et al. (2002) based on Seasoar data. We are not aware of observational evidence for the South Pacific Ocean to concur with the present study. No region of density compensation was found in the Atlantic Ocean, although there have been observations of compensation there previously (Roden 1986). However, our investigation covered in detail only the Subtropical Front, and other frontal regions might well be density-compensated. One candidate for density compensation in the Atlantic Ocean is the Cape Verde Frontal Zone. This front, created by the meeting of North Atlantic and South Atlantic Central Water, has been observed to be nearly density-compensated (Klein and Siedler 1995). An indication of this can be seen in the meridional Turner angle distribution at 300 m depth (Fig. 3), which shows a narrow band of low Turner angles near the West African coast at 20°N.

The only region of the world ocean where the STF is density-compensated below the mixed layer is found in the eastern Indian Ocean south of Australia. James et al. (2002) recently identified this region as an area where east of 135°E the STF is nearly fully density-compensated and tends to break up into filaments and swirls dominated by inversions and extended sheets of water with different TS properties. They point out that the change in character of the STF from Africa to the area south of the Great Australian Bight has important consequences for the frontal current system. Stramma (1992) describes the STF from Africa to western Australia as a frontal system associated with significant geostrophic flow, which he calls the South Indian Ocean Current. He estimates the transport of this current as 60 Sv ($1\ \mathrm{Sv} = 10^6\ \mathrm{m^3 s^{-1}}$) east of Africa, 20 Sv near 70°E and 10 Sv west of southwestern Australia. Schodlock et al. (1997) follow this current further to the east and show evidence that it does not reach beyond 120°E. Yet the Subtropical Front persists. The lack of a strong associated frontal current allows processes such as double diffusion and interleaving to develop undisturbed and change the structure and appearance of the front.

The detailed identification of frontal regions with nearly complete density compensation is a task for the future. There are indications that parts of the fronts of the Southern Ocean – the backbone of the Circumpolar Current System – are highly density-compensated (Roden 1986). How do they maintain their large transports in a density-compensated environment? Does density compensation change their mixing characteristics? Does it influence the probability of eddy shedding, or is this only a function of interaction with bottom topography? The methodology of this study, which rests on the presence of significant horizontal TS gradients, is not well tailored to investigate the Southern Ocean.

A clear result of the present study is the fact that different oceans have different preferred meridional Turner angles and associated density ratios (Table 1). Stommel's (1993) canonical value $R_\rho^{hy} = 2$ is common – it is found at 300 m in the STF of the South Atlantic and of the South Indian Ocean and seasonally in the mixed layer of all oceans – but not unique. The thermocline of the North Pacific Ocean is characterized in both hemispheres by $R_\rho^{hy} = 3.2$ and the North Atlantic thermocline by $R_\rho^{hy} = 1.6$. Explanations for these differences are likely to be found in the different atmospheric conditions over the three oceans.

Acknowledgement We thank Dan Rudnick for helpful comments and discussion during the preparation of this paper.

References

Belkin IM, Gordon AL (1996) Southern Ocean fronts from the Greenwich meridian to Tasmania. J Geophys Res 101: 3675–3696

Chen LG (1995) Mixed layer density ratio from the Levitus data. J Phys Oceanogr 25: 691–701

Conkright M, Levitus S, O'Brien T, Boyer T, Antonov J, Stephens C (1998) World Ocean Atlas 1998 CD-ROM Dataset documentation. Tech Rep **15** NODC Internal Report

Ferrari R, Young WR (1997) On the development of thermohaline correlations as a result of nonlinear diffusive parameterizations. J Mar Res 55: 1069–1101

Figueroa HA (1996) World ocean density ratios. J Phys Oceanogr 26: 267–275

Gordon A, Grace W, Schwerdtfeger P, Byron-Scott R (1998) Dynamic meteorology: a basic course. Arnold, London

Kazmin AS, Rienecker MM (1996) Variability and frontogenesis in the large-scale oceanic frontal zones. J Geophys Res 101: 907–921

James C, Tomczak M, Helmond I, Pender L (2002) Summer and winter surveys of the Subtropical Front of the southeastern Indian Ocean. J Mar Systems 37: 129–149

Klein B, Siedler G (1995) Isopycnal and diapycnal mixing at the Cape Verde Frontal Zone. J Phys Oceanogr 25: 1771–1787

Levitus S (1982) Climatological atlas of the world ocean. NOAA Prof. Paper No. 13

Niiler PP, Reynolds RW (1984) The three-dimensional circulation near the eastern North Pacific Subtropical Front. J Phys Oceanogr 14: 217–230

Roden GI (1975) On North Pacific temperature, salinity, sound velocity and density fronts and their relation to the wind and energy flux fields. J Phys Oceanogr 5: 557–571

Roden GI (1977) Oceanic Subarctic Fronts of the Central Pacific: structure of and response to atmospheric forcing. J Phys Oceanogr 7: 761–778

Roden GI (1980a) On the subtropical frontal zone north of Hawaii during winter. J Phys Oceanogr 10: 342–362

Roden GI (1980b) On the variability of sea-surface temperature fronts in the western Pacific, as detected by satellite. J Geophys Res 85: 2704–2710

Roden GI (1986) Thermohaline fronts and baroclinic flow in the Argentine Basin during the austral spring of 1984. J Geophys Res 91: 5075–5093

Ruddick B (1983) A practical indicator of the stability of the water column to double diffusive activity. Deep-Sea Res 30: 1105–1107

Rudnick DL, Ferrari R (1999) Compensation of horizontal temperature and salinity gradients in the ocean mixed layer. Science 283: 526–529

Rudnick DL, Martin JP (2002) On the horizontal density ratio in the upper ocean. Dyn Atmos Oceans 36: 3–23

Schmitt RW (1999) Spice and the demon. Science 283: 498–499

Schodlock MP, Tomczak M, White N (1997) Deep sections through the South Australian Basin and across the Australian–Antarctic Discordance. Geophys Res Letters 24: 2785–2788

Stommel HM (1993) A conjectural regulating mechanism for determining the thermohaline structure of the oceanic mixed layer. J Phys Oceanogr 23: 142–148

Stramma L (1992) The South Indian ocean current. J Phys Oceanogr 22: 421–430

Tomczak M (1977) Continuous measurement of near-surface temperature and salinity in the NW African upwelling region between Canary Islands and Cape Vert during the winter of 1971–1972. Deep-Sea Res 24: 1103–1119

Tomczak M, Gu YH (1987) Water mass properties of the permanent thermocline in the western South Pacific Ocean during WESTROPAC '82. Deep-Sea Res 34: 1713–1731

Tomczak M, Godfrey JS (1994) Regional oceanography: an Introduction. Pergamon

You Y, Tomczak M (1993) Thermocline circulation and ventilation in the Indian Ocean derived from water mass analysis. Deep-Sea Res 40: 13–56

Yuan X, Talley LD (1992) Shallow salinity minima in the North Pacific. J Phys Oceanogr 22: 1302–1316